Available online at www.sciencedirect.com

ScienceDirect

Procedia IUTAM 11 (2014) 58 – 68

Procedia IUTAM

www.elsevier.com/locate/procedia

Nonlinear Interfacial Wave Phenomena from the Micro- to the Macro-Scale

Electrostatic effects on linear and nonlinear waves in hanging film flows

M. Hunt[a], D.T. Papageorgiou[b], J.-M. Vanden-Broeck[a,*]

[a] *Department of Mathematics, University College London, London WC1E 6BT, U.K.*
[b] *Department of Mathematics, Imperial College London, London SW7 2AZ, U.K.*

Abstract

The dynamics of a liquid film wetting the underside of a semi-infinite horizontal substrate are investigated. Gravity causes the film to be unstable and the objective of this work is to control such instabilities by using horizontal electric fields. The film wets a semi-infinite dielectric solid block and is bounded below by air. The electric fields from these two regions are coupled to those in the liquid film and contribute to the hydrodynamics through the interfacial boundary conditions by introducing electric Maxwell stresses in the stress tensor. As a result novel nonlocal terms arise and their effect is studied both in the linear regime as well as nonlinearly through a derivation of a system of long-wave one-dimensional evolution equations describing the interfacial position and the leading order horizontal velocity in the film. When surface tension is present there exists a band of unstable wavenumbers rendering the film long-wave unstable. It is shown that the size of this band decreases asymptotically to zero as the electric field strength is increased (physically this means that any system of finite horizontal length can be fully stabilized by a sufficiently strong electric field). The derived nonlinear system supports nonlinear coherent structures in the form of traveling waves of permanent form, and such solutions are computed numerically for a range of parameters. The production of such traveling waves may be useful in enhancing the transport properties in hanging film systems.

Selection and peer-review under responsibility of scientific committee of Nonlinear Interfacial Wave Phenomena from the Micro- to the Macro-Scale

Keywords: Liquid films; electrostatic stabilization; nonlinear waves.

1. Introduction

Thin liquid films are ubiquitous in technological, biophysical and biological applications, and have been the subject of extensive research in recent years (the subject along with numerous applications has been reviewed [1,2]). Instabilities and ensuing nonlinear dynamics in thin liquid films can arise due to different physical mechanisms including, among others, shear-induced instabilities (e.g. inertial instabilities in falling liquid films above a threshold Reynolds number [3,4]), interfacial instabilities due to surface tension variations (Marangoni instabilities [1,2]), gravitational instabilities (Rayleigh-Taylor), as well as instabilities induced by external electric fields [5,6,7]. More recent work on electrified film-flow over topograpically structured substrates has revealed that appropriately chosen topography can destabilize

* Corresponding author. Tel.: + 44 (0) 2076792835 ; fax: +44 (0) 2073835519.
E-mail address: j.vanden-broeck@ucl.ac.uk

Selection and peer-review under responsibility of scientific committee of Nonlinear Interfacial Wave Phenomena from the Micro- to the Macro-Scale
doi:10.1016/j.piutam.2014.01.048

or stabilize the flow[8], but also that electric fields can be utilized to reduce the sizes of interfacial ridges encountered in film-flow down steps[9,10,11,12].

The present work is concerned with the interaction between an imposed electric field and Rayleigh-Taylor gravitational instabilities. The fundamental problem considered is that of a hanging film where a liquid layer coats the underside of a horizontal substrate so that it is unstable due to the presence of gravity. We are interested in controlling such instabilities via the application of a horizontal electric field (i.e. acting parallel to the undisturbed flat interface). The feasibility of such stabilization has been demonstrated theoretically for a film wetting the underside of the top boundary of a horizontal channel[13]. Direct numerical simulations of the Navier-Stokes equations at both small and moderate Reynolds numbers, also confirm that the Rayleigh-Taylor instability can be suppressed by sufficiently strong electric fields acting parallel to the undisturbed interface[14]. We note that if the field is perpendicular to the undisturbed interface, then it will cause destabilization above a critical value[6], a phenomenon that was originally identified and described by G.I. Taylor[15]. The present work extends the analysis of Barannyk et al.[13] who used insulating boundary conditions for the voltage at solid walls, in order to produce a model that is closer to experimental situations. We incorporate the electrodynamics of the upper solid whose underside is wetted by the liquid film. This upper solid is typically a perspex block and we take it to be of infinite lateral extent (this is a reasonable assumption since the liquid layer is thin - there is numerical evidence for the insensitivity of solutions on truncations of such regions[14]). As a result the voltage potential needs to be solved in the upper solid region as well as in the liquid film and the lower air region below the film. The resulting equations inherit nonlocal terms due to the solutions in these unbounded regions resulting in novel evolution equations.

The paper is organized as follows. Section 2 presents the mathematical statement of the full problem along with the exact nonlinear boundary conditions. Section 3 presents the linear stability properties of the flow about the flat uniform states, while Section 4 is devoted to the long-wave asymptotic analysis that is used to derive a reduced system of evolution PDEs governing the flow in this limit. Section 5 solves these PDEs numerically and in particular nonlinear traveling waves are constructed. In Section 6 we present our conclusions.

2. Mathematical formulation

We consider an inviscid incompressible perfect dielectric fluid wetting the underside of a horizontal ceiling wall. The fluid has density ρ and undisturbed thickness h (see Figure 1). The configuration is assumed to be two-dimensional and using the usual Cartesian coordinate system, the upper bounding wall is located at $y = h$, the undisturbed interface at $y = 0$, and the evolving interface at $y = \eta(x,t) < h$. The region $y < \eta(x,t)$ below the interface is a gas (typically air) and the region $y > h$ is solid. The variables in the fluid, solid and gas regions will be distinguished by letters f, s and g, respectively. The corresponding dielectric permittivities are ϵ_f, ϵ_s and ϵ_g. In addition to the presence of gravity acting vertically downwards with acceleration g, a horizontal electric field acts with uniform value E_0 far away.

The electrostatic limit of Maxwell's equations is appropriate and the electric fields can be represented by voltage potentials as $\boldsymbol{E}^{f,s,g} = -\nabla V^{f,s,g}$, and these satisfy the Laplace equations

$$\nabla^2 V^s = 0, \qquad y > h, \tag{1}$$

$$\nabla^2 V^f = 0, \qquad \eta < y < h, \tag{2}$$

$$\nabla^2 V^g = 0, \qquad y < \eta. \tag{3}$$

The flow is assumed irrotational so that the velocity vector is given by $\boldsymbol{u} = \nabla\phi$ where ϕ is the velocity potential and due to incompressibility it also satisfies Laplace's equation

$$\nabla^2 \phi = 0, \qquad \eta < y < h. \tag{4}$$

The electric field boundary conditions at $y = h$ and $y = \eta(x,t)$, are the continuity of the tangential component $\boldsymbol{t}\cdot\boldsymbol{E}$ of the electric field and the continuity of the normal component of the electric displacement $\epsilon\boldsymbol{E}\cdot\boldsymbol{n}$ (here $\boldsymbol{t} = (1,\eta_x)/\sqrt{1+\eta_x^2}$,

and $\boldsymbol{n} = (-\eta_x, 1)/\sqrt{1+\eta_x^2}$ are the unit tangent and normal at interfaces). These equations are

$$V^s = V^f, \qquad \epsilon_s \frac{\partial V^s}{\partial y} = \epsilon_f \frac{\partial V^f}{\partial y}, \qquad \text{at } y = h \tag{5}$$

$$\frac{\partial V^f}{\partial x} + \frac{\partial \eta}{\partial x}\frac{\partial V^f}{\partial y} = \frac{\partial V^g}{\partial x} + \frac{\partial \eta}{\partial x}\frac{\partial V^g}{\partial y}, \quad \text{at } y = \eta \tag{6}$$

$$\epsilon_f\left(-\frac{\partial \eta}{\partial x}\frac{\partial V^f}{\partial x} + \frac{\partial V^f}{\partial y}\right) = \epsilon_g\left(-\frac{\partial \eta}{\partial x}\frac{\partial V^g}{\partial x} + \frac{\partial V^g}{\partial y}\right), \quad \text{at } y = \eta. \tag{7}$$

Far away we must impose

$$V^s \sim -E_0 x, \quad \text{as } y \to \infty, \tag{8}$$

$$V^g \sim -E_0 x, \quad \text{as } y \to -\infty. \tag{9}$$

The hydrodynamic boundary conditions are a no penetration condition at the wall $\phi_y(x, h, t) = 0$, a kinematic condition at the interface

$$\frac{\partial \eta}{\partial t} + \frac{\partial \phi}{\partial x}\frac{\partial \eta}{\partial x} = \frac{\partial \phi}{\partial y}, \qquad \text{at } y = \eta(x, t), \tag{10}$$

and the following electrically modified dynamic Bernoulli condition [16] at $y = \eta(x, t)$

$$\frac{\partial \phi}{\partial t} + \frac{1}{2}|\nabla\phi|^2 + g\eta + \frac{1}{\rho}\frac{1}{(1+\eta_x^2)}\left((\eta_x^2 - 1)[\mathcal{E}_{11}]_g^f + 2\eta_x[\mathcal{E}_{12}]_g^f\right) = -\frac{\sigma}{\rho}\frac{\eta_{xx}}{(1+\eta_x^2)^{3/2}} + C, \tag{11}$$

where σ is the coefficient of surface tension and

$$\mathcal{E}_{11} = \frac{\epsilon}{2}(V_x^2 - V_y^2), \qquad \mathcal{E}_{12} = \epsilon V_{xy}. \tag{12}$$

The boundary conditions (5) coupling regions f and s are most usefully cast into a single boundary condition for V^f by utilising the fact that V^s is a harmonic function. Writing $V^f = -x + \tilde{V}^f$, $V^s = -x + \tilde{V}^s$ and since $\tilde{V}^s$ is harmonic, we have at the wall

$$\partial_x \tilde{V}^s(x, h) = \mathcal{H}(\partial_y \tilde{V}^s(x, h)), \qquad \partial_y \tilde{V}^s(x, h) = -\mathcal{H}(\partial_x \tilde{V}^s(x, h)), \tag{13}$$

where $\mathcal{H}(f) = \frac{1}{\pi} PV \int_{-\infty}^{\infty} \frac{f(\theta)}{x-\theta} d\theta$ is the Hilbert transform of the function $f(x)$; of particular relevance to us is the Fourier symbol of this operator, namely $\widehat{\mathcal{H}f} = -i\mathrm{sgn}(k)\hat{f}(k)$ where k is the wavenumber and hats denote the usual Fourier transform. The first condition in (5) can be written as $\partial_x \tilde{V}^s = \partial_x \tilde{V}^f$, while the second condition becomes (using (13))

$$\varepsilon_f \partial_y \tilde{V}^f = -\varepsilon_s \mathcal{H}(\partial_x \tilde{V}^s) \quad \Rightarrow \quad \varepsilon_f \partial_y \tilde{V}^f = -\varepsilon_s \mathcal{H}(\partial_x \tilde{V}^f). \tag{14}$$

The non-local boundary condition (14) can be imposed as a single condition for the field $\tilde{V}^f$ at the wall and this is used later in Section 4.

The problem formulated above is a nonlinear free boundary problem and we proceed analytically by studying linear aspects first before providing a weakly nonlinear theory.

3. Linear stability

The model given in Section 2 is non-dimensionalized by using h, $\sqrt{\frac{\rho h^3}{\sigma}}$, $E_0 h$ as reference length, time, and electric potential, respectively. We consider perturbations to the steady state of the form

$$V^{f,s,g} = -x + \delta\, v^{f,s,g}, \quad \phi = \delta\, \varphi^{f,s,g}, \quad \eta = \delta\, S, \tag{15}$$

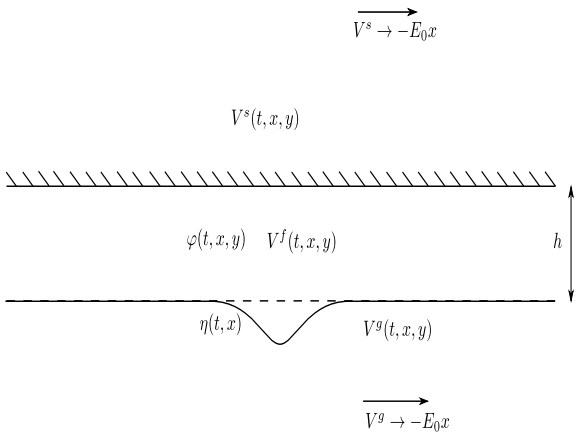

Fig. 1. Schematic of the problem. A liquid layer (region f) wets the underside of the dielectric half-space (region s) with a gas half-space below it (region g). A horizontal field is applied as shown.

where δ is a small parameter allowing linearization around the undisturbed state. Substituting into the dimensionless governing equations and boundary conditions, and keeping terms of order δ alone, yields the following linear system

$$\nabla^2 v^s = 0, \qquad y > 1, \tag{16}$$

$$\nabla^2 v^f = 0, \qquad 0 < y < 1, \tag{17}$$

$$\nabla^2 v^g = 0, \qquad y < 0, \tag{18}$$

$$\nabla^2 \varphi = 0, \qquad 0 < y < 1, \tag{19}$$

and corresponding boundary conditions

$$v^s = v^f, \qquad \epsilon_{s,f} \frac{\partial v^s}{\partial y} = \frac{\partial v^f}{\partial y}, \qquad \text{at } y = 1 \tag{20}$$

$$v^f = v^g, \qquad (\epsilon_{f,g} - 1)\frac{\partial S}{\partial x} + \epsilon_{f,g}\frac{\partial v^f}{\partial y} - \frac{\partial v^g}{\partial y} = 0 \quad \text{at } y = 0, \tag{21}$$

$$\frac{\partial S}{\partial t} = \frac{\partial \varphi}{\partial y} \qquad \text{at } y = 0 \tag{22}$$

$$\frac{\partial \varphi}{\partial y} = 0 \qquad \text{at } y = 1 \tag{23}$$

$$\frac{\partial^2 \varphi}{\partial t \partial x} + B\frac{\partial S}{\partial x} + \epsilon_{f,g} E_b \frac{\partial^2 v^f}{\partial x^2} - E_b \frac{\partial^2 v^g}{\partial x^2} + \frac{\partial^3 S}{\partial x^3} = 0, \qquad \text{at } y = 0. \tag{24}$$

The dimensionless parameters appearing are given

$$\epsilon_{s,f} = \frac{\epsilon_s}{\epsilon_f}, \quad \epsilon_{f,g} = \frac{\epsilon_f}{\epsilon_g}, \quad B = \frac{\rho g h^2}{\sigma}, \quad E_b = \frac{E_0^2 \epsilon_g h}{\sigma}, \tag{25}$$

and denote permittivity ratios between the phases, the Bond number and an electric Weber number.

This linear system is solved by separation of variables with solutions proportional to $e^{ikx - i\omega t}$, where k is the wavenumber (assumed real) and ω is an eigenvalue to be determined. After some algebra, we obtain for $k > 0$

$$c^2 = \frac{\omega^2}{k^2} = \left[k^2 - B + \frac{k E_b (\epsilon_{f,g} - 1)^2 (1 + \epsilon_{s,f} + (1 - \epsilon_{s,f}) e^{-2k})}{(1 + \epsilon_{s,f})(1 + \epsilon_{f,g}) + (1 - \epsilon_{s,f})(1 - \epsilon_{f,g}) e^{-2k}} \right] \frac{\tanh k}{k}. \tag{26}$$

Note that the flow is stable when c^2 is positive and unstable when it is negative. It can be seen that short waves are always stable since $c^2 \sim k$ for large k, whereas sufficiently long waves are unstable since

$$c^2 \sim -B + k \frac{E_b (\epsilon_{f,g} - 1)^2}{1 + \epsilon_{s,f} \epsilon_{f,g}} + \ldots. \tag{27}$$

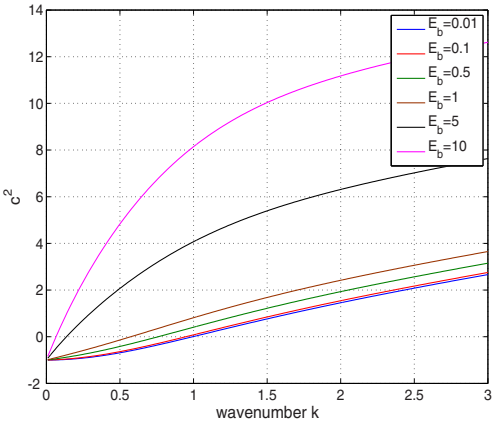

Fig. 2. Linear dispersion relation (26) as the electric field strength parameter E_b varies from small to large values as shown in the legend. Other parameters are $B = 1$, $\epsilon_{s,f} = 0.5$, $\epsilon_{f,g} = 3$. The band of instability decreases as E_b increases.

The variation of c^2 with wavenumber k for a large range of values of E_b is included in Fig. 2. The left panel corresponds to small values of E_b ranging from 0.01 to 0.5, while the right panel includes E_b values ranging from 0.5 to 3.0. It can be seen that as the applied electric field increases the band of unstable waves in the vicinity of $k = 0$, decreases significantly. From a practical viewpoint we note that if the system has a fixed horizontal extent (e.g. a channel of low aspect ratio but finite horizontal extent) then a large enough E_b will suppress the Rayleigh-Taylor instability to waves that are longer than the system size. This observation could be particularly useful in experiments (see [14] for direct numerical simulations along with a physical example).

4. Nonlinear long wave theory

4.1. Formulation and non-dimensionalisation

In this section we consider nonlinear dynamics valid for waves which are long compared to the undisturbed layer depth h. To achieve this we consider the dimensional system (1)-(4) along with the interfacial boundary conditions (5)-(11), and non-dimensionalise as follows:

$$x = L\,\hat{x}, \qquad y^s = L\,\hat{y}, \qquad y^g = L\,Y, \qquad y^f = h(1+\zeta), \qquad \eta = h\,\hat{\eta}, \tag{28}$$

where L is a typical horizontal length scale and ζ is a vertical coordinate in the fluid layer and has been chosen so that the wall is at $\zeta = 0$ and the interface is at $\zeta = -1 + \hat{\eta}$. In addition we non-dimensionalise time, and the fluid and voltage potentials by

$$t = \sqrt{\frac{\rho L^3}{\sigma}}\,\hat{t}, \qquad \phi = \sqrt{\frac{\sigma L}{\rho}}\,\hat{\varphi}, \qquad V = E_0 L\,\hat{V}. \tag{29}$$

In what follows we assume that $\delta = h/L$ is a small parameter and use this to develop asymptotic expansions to solve the problem. Substituting these scalings into the governing equations and boundary conditions, and dropping hats from dependent variables, we obtain

$$\frac{\partial^2 V^f}{\partial \hat{x}^2} + \frac{1}{\delta^2}\frac{\partial^2 V^f}{\partial \zeta^2} = 0, \qquad -1+\eta < \zeta < 0, \tag{30}$$

$$\frac{\partial^2 V^g}{\partial \hat{x}^2} + \frac{\partial^2 V^g}{\partial Y^2} = 0, \qquad Y < \delta\eta, \tag{31}$$

$$\frac{\partial^2 \varphi}{\partial \hat{x}^2} + \frac{1}{\delta^2}\frac{\partial^2 \varphi}{\partial \zeta^2} = 0, \qquad -1+\eta < \zeta < 0. \tag{32}$$

The non-local electric field boundary condition (14) at the wall becomes

$$\partial_\zeta \tilde{V}^f = -\epsilon_{s,f}\,\delta\,\mathcal{H}(\partial_{\hat{x}}\tilde{V}^f) \qquad \text{at} \qquad \zeta = 0, \tag{33}$$

where we recall the definition $V^f = -\hat{x} + \tilde{V}^f$, and it is understood that the Hilbert transform in (33) is an integral with respect to $\hat{x}$. The corresponding boundary conditions at the interface read

$$\frac{\partial V^f}{\partial \hat{x}} + \frac{\partial \eta}{\partial \hat{x}}\frac{\partial V^f}{\partial \zeta} = \frac{\partial V^g}{\partial \hat{x}} + \delta\frac{\partial \eta}{\partial \hat{x}}\frac{\partial V^g}{\partial Y}, \tag{34}$$

$$\epsilon_{f,g}\left(-\delta\frac{\partial \eta}{\partial \hat{x}}\frac{\partial V^f}{\partial \hat{x}} + \frac{1}{\delta}\frac{\partial V^f}{\partial \zeta}\right) = -\delta\frac{\partial \eta}{\partial \hat{x}}\frac{\partial V^g}{\partial \hat{x}} + \frac{\partial V^g}{\partial Y}. \tag{35}$$

The permittivity ratios appearing in (33) and (35) are as defined in (25). The far field conditions (8)-(9) become $V^s \sim -\hat{x}$, $V^g \sim -\hat{x}$. For the fluid potential the no penetration condition at the wall $\zeta = 0$ becomes $\varphi_\zeta = 0$, while the kinematic boundary condition (10) at the interface $\zeta = -1 + \eta$ becomes

$$\delta\frac{\partial \eta}{\partial \hat{t}} + \delta\frac{\partial \varphi}{\partial \hat{x}}\frac{\partial \eta}{\partial \hat{x}} = \frac{1}{\delta}\frac{\partial \varphi}{\partial \zeta}. \tag{36}$$

Finally, the Bernoulli equation (11) becomes

$$\frac{\partial \varphi}{\partial \hat{t}} + \frac{1}{2}\left[\left(\frac{\partial \varphi}{\partial \hat{x}}\right)^2 + \frac{1}{\delta^2}\left(\frac{\partial \varphi}{\partial \zeta}\right)^2\right] + \delta B\eta + \frac{E_b Q}{1+\delta^2\eta_{\hat{x}}^2} = -\frac{\delta\eta_{\hat{x}\hat{x}}}{(1+\delta^2\eta_{\hat{x}}^2)^{3/2}} + C, \tag{37}$$

where

$$Q = \delta^2\eta_{\hat{x}}^2(\epsilon_{f,g}M_{11}^f - M_{11}^g) - 2\delta\eta_{\hat{x}}(\epsilon_{f,g}M_{12}^f - M_{12}^g) - \epsilon_{f,g}M_{11}^f + M_{11}^g, \tag{38}$$

with

$$M_{11}^f = \frac{1}{2}\left[\left(\frac{\partial V^f}{\partial \hat{x}}\right)^2 - \frac{1}{\delta^2}\left(\frac{\partial V^f}{\partial \zeta}\right)^2\right], \qquad M_{12}^f = \frac{1}{\delta}\frac{\partial^2 V^f}{\partial \hat{x}\partial\zeta}, \tag{39}$$

$$M_{11}^g = \frac{1}{2}\left[\left(\frac{\partial V^g}{\partial \hat{x}}\right)^2 - \left(\frac{\partial V^g}{\partial Y}\right)^2\right], \qquad M_{12}^g = \frac{\partial^2 V^g}{\partial \hat{x}\partial Y}. \tag{40}$$

The scaled system presented above is exact but contains the small parameter δ, enabling an asymptotic solution to be sought for $\delta \ll 1$ as we describe next.

4.2. Asymptotic expansions

The appropriate asymptotic expansions are

$$\varphi(\hat{x},\zeta,\hat{t}) = \delta^{1/2}\left(\varphi_0 + \delta^2\varphi_1 + \ldots\right), \tag{41}$$

$$\eta(\hat{x},\hat{t}) = \eta_0 + \delta^2\eta_1 + \ldots, \tag{42}$$

$$V^f(\hat{x},\zeta,\hat{t}) = -\hat{x} + \delta\left(V_1^f + \delta V_2^f + \ldots\right), \tag{43}$$

$$V^g(\hat{x},Y,\hat{t}) = -\hat{x} + \delta\left(V_1^g + \delta V_2^g + \ldots\right). \tag{44}$$

Note that the $\delta^{1/2}$ scaling for φ is chosen in order to balance nonlinear terms with surface tension in the Bernoulli equation (37) (an appropriate related time-scale is needed as we shall see below). In addition, the expansion for φ proceeds in powers of δ^2 while those for $V^{f,g}$ proceed in powers of δ; the reason is that in the former case the equations and boundary conditions contain δ^2 as a small parameter while in the case of the voltage potentials δ appears in the nonlocal boundary condition (33). Inserting these expansions into the governing equations and boundary conditions

yields a sequence of problems to solve at each order. Starting with the fluid layer, the Laplace equation (32) for the fluid potential gives at the first two orders $O(\delta^{-3/2})$ and $O(\delta^{1/2})$, respectively

$$\frac{\partial^2\varphi_0}{\partial\zeta^2} = 0, \tag{45}$$

$$\frac{\partial^2\varphi_1}{\partial\zeta^2} + \frac{\partial^2\varphi_0}{\partial\hat{x}^2} = 0. \tag{46}$$

These are readily integrated and on applying the no penetration boundary condition at the wall $\zeta = 0$ we have $\varphi_{0\zeta}|_{\zeta=0} = \varphi_{1\zeta}|_{\zeta=0} = 0$, hence

$$\varphi_0 \equiv \varphi_0(x,t), \tag{47}$$

$$\varphi_1 = -\frac{1}{2}\zeta^2\varphi_{0\hat{x}\hat{x}} + A(\hat{x},\hat{t}), \tag{48}$$

where the functions $\varphi_0(\hat{x},\hat{t})$ and $A(\hat{x},\hat{t})$ are to be determined.

The first evolution equation now follows from the leading order contribution of the scaled kinematic condition (36) evaluated at $\zeta = -1+\eta_0$. Noting that the second and third terms of (36) are of order $\delta^{3/2}$, it follows that a balance is possible if a new slow time-scale τ is introduced by writing $\hat{t} = \tau/\delta^{1/2}$. The resulting equation is

$$\frac{\partial\eta_0}{\partial\tau} + \frac{\partial\varphi_0}{\partial\hat{x}}\frac{\partial\eta_0}{\partial\hat{x}} = -(\eta_0-1)\frac{\partial^2\varphi_0}{\partial\hat{x}^2} \qquad \Rightarrow \qquad \frac{\partial\eta_0}{\partial\tau} + \frac{\partial}{\partial\hat{x}}\left((\eta_0-1)\frac{\partial\varphi_0}{\partial\hat{x}}\right) = 0. \tag{49}$$

The second equation is provided by the leading order terms of the Bernoulli equation (37). In order to calculate the electrostatic Maxwell stress contributions we begin by solving for the voltage potentials in regions f and g. Substituting expansions (42)-(44) into equations (30)-(31), and keeping leading order terms provides

$$\frac{\partial^2 V_1^f}{\partial\zeta^2} = 0, \qquad \frac{\partial^2 V_2^f}{\partial\zeta^2} = 0, \qquad -1+\eta_0 < \zeta < 0, \tag{50}$$

$$\frac{\partial^2 V_1^g}{\partial\hat{x}^2} + \frac{\partial^2 V_1^g}{\partial Y^2} = 0, \qquad Y < 0. \tag{51}$$

Equations (50) are readily solved to find

$$V_1^f = A_1(\hat{x},\tau)\zeta + B_1(\hat{x},\tau), \qquad V_1^f = A_2(\hat{x},\tau)\zeta + B_2(\hat{x},\tau) \tag{52}$$

where the functions $A_{1,2}(\hat{x},\tau), B_{1,2}(\hat{x},\tau)$ are to be found. At $O(1)$ and $O(\delta)$ the nonlocal boundary condition (33) gives

$$\partial_\zeta V_1^f = 0, \qquad \partial_\zeta V_2^f = -\epsilon_{s,f}\,\mathcal{H}(\partial_{\hat{x}} V_1^f), \tag{53}$$

hence $A_1 \equiv 0$ and

$$V_1^f \equiv B_1(\hat{x},\tau), \qquad A_2 = -\epsilon_{s,f}\mathcal{H}(\partial_{\hat{x}} B_1). \tag{54}$$

Note that B_2 is undetermined but of no relevance since it is the vertical electric field $\partial_\zeta V^f$ that is needed in the completion of the asymptotic solution.

Equation (51) can be solved by introducing the Fourier transform pair $\widehat{g}(k) = \int_{-\infty}^{\infty} g(x)e^{-ik\hat{x}}d\hat{x}$, $g(x) = \frac{1}{2\pi}\int_{-\infty}^{\infty}\widehat{g}(k)e^{ik\hat{x}}dk$ for square integrable functions, and using the boundary condition that the field is uniform as $Y \to -\infty$ to obtain

$$\widehat{V_1^g}(k,Y,\tau) = \alpha(k,\tau)\,e^{|k|\hat{Y}}. \tag{55}$$

We note that $\widehat{V_{1Y}^g}\big|_{Y=0} = \alpha\,|k|$, and this is used below.

It remains to determine the unknown functions B_1 and α in terms of the interfacial shape η_0 in order to obtain the final required form of the Bernoulli equation. This information comes from the electrostatic interfacial conditions (34)-(35) that correspond to continuity of the electric potential and the electric displacement, respectively. Substitution

of (42)-(44) into (34)-(35), and retention of leading order terms yields (note that these are at order δ in both boundary conditions since the order one undisturbed electric field terms cancel in (34))

$$\left.\frac{\partial V_1^f}{\partial \hat{x}}\right|_{\zeta=-1+\eta_0} = \left.\frac{\partial V_1^g}{\partial \hat{x}}\right|_{Y=0}, \tag{56}$$

$$\epsilon_{f,g}\frac{\partial \eta_0}{\partial \hat{x}} - \epsilon_{f,g}\,\epsilon_{s,f}\,\mathcal{H}(B_{1\hat{x}}) = \frac{\partial \eta_0}{\partial \hat{x}} + \left.\frac{\partial V_1^g}{\partial Y}\right|_{Y=0}. \tag{57}$$

Using the solutions (54) and (55) and taking the Fourier transforms of (56) and (57), gives

$$\widehat{B_1} = \alpha, \tag{58}$$

$$ik(\epsilon_{f,g}-1)\widehat{\eta_0} = \alpha|k| + \epsilon_{f,g}\,\epsilon_{s,f}|k|\widehat{B_1}, \tag{59}$$

so that

$$\widehat{B_1} = \alpha = i\mathrm{sgn}(k)\,\frac{(\epsilon_{f,g}-1)}{(1+\epsilon_{f,g}\,\epsilon_{s,f})}\,\widehat{\eta_0}. \tag{60}$$

With these results we are now in a position to find the leading order electrostatic contribution Q in the scaled Bernoulli equation (37). Inspection of (38)-(40) along with the asymptotic solutions found above shows that

$$Q = \frac{1}{2}(1-\epsilon_{f,g}) + \delta(\epsilon_{f,g}B_{\hat{x}} - V_{1\hat{x}}^g) + O(\delta^2). \tag{61}$$

Considering the scaled Bernoulli equation (37), introducing the asymptotic expansions (41)-(44) along with the slow time-scale $\hat{t} = \tau/\delta^{1/2}$ introduced earlier and the asymptotic solutions (47)-(48) for the fluid potential shows that the leading order non-constant terms in the equation are of order δ so that hydrodynamic and electrostatic effects are in balance. It is convenient to differentiate (37) with respect to $\hat{x}$ and to introduce the leading order horizontal velocity

$$u = \frac{\partial \varphi_0}{\partial \hat{x}}, \tag{62}$$

to find the following evolution equation

$$\frac{\partial u}{\partial \tau} + u\frac{\partial u}{\partial \hat{x}} + B\frac{\partial \eta_0}{\partial \hat{x}} + E_b(\epsilon_{f,g}B_1 - V_1^g)_{\hat{x}\hat{x}} = -\frac{\partial^3 \eta_0}{\partial \hat{x}^3}. \tag{63}$$

Defining $Q_1 = (\epsilon_{f,g}B_1 - V_1^g)_{\hat{x}\hat{x}}$ and taking the Fourier transform, we find

$$\widehat{Q_1} = -k^2(\epsilon_{f,g}\widehat{B_1} - \alpha) = -i\mathrm{sgn}(k)\,k^2\frac{(\epsilon_{f,g}-1)^2}{(1+\epsilon_{f,g}\,\epsilon_{s,f})}\widehat{\eta_0}. \tag{64}$$

Using the Hilbert transform introduced earlier along with its symbol in Fourier space, we can conclude that

$$Q_1 = -\frac{(\epsilon_{f,g}-1)^2}{(1+\epsilon_{f,g}\,\epsilon_{s,f})}\mathcal{H}[\eta_{0\hat{x}\hat{x}}]. \tag{65}$$

To summarize, then, we have obtained the following coupled system of evolution equations for η_0 and $u = \frac{\partial \phi_0}{\partial \hat{x}}$

$$\frac{\partial \eta_0}{\partial \tau} + \frac{\partial}{\partial \hat{x}}\left((\eta_0 - 1)u\right) = 0, \tag{66}$$

$$\frac{\partial u}{\partial \tau} + u\frac{\partial u}{\partial \hat{x}} + B\frac{\partial \eta_0}{\partial \hat{x}} - E_b\frac{(\epsilon_{f,g}-1)^2}{(1+\epsilon_{f,g}\,\epsilon_{s,f})}\mathcal{H}[\eta_{0\hat{x}\hat{x}}] = -\frac{\partial^3 \eta_0}{\partial \hat{x}^3}. \tag{67}$$

Before proceeding to presenting numerical solutions of the system (66)-(67) we consider linear properties. Linearising about the uniform state $(\eta_0, u) = (0, 0)$ and looking for solutions proportional to $e^{ik\hat{x}-i\omega\tau}$ yields the dispersion relation

$$\omega^2 = -k^2\,B + k^2\,|k|\,\frac{E_b(\epsilon_{f,g}-1)^2}{(1+\epsilon_{s,f}\epsilon_{f,g})} + k^4. \tag{68}$$

Hence,

$$c^2 = \frac{\omega^2}{k^2} = -B + |k|\frac{E_b(\epsilon_{f,g}-1)^2}{(1+\epsilon_{s,f}\epsilon_{f,g})} + k^2, \tag{69}$$

and this is in complete agreement with the long-wave expansion of the exact dispersion relation (26) given in (27).

5. Nonlinear traveling waves

We first rewrite the system (66)-(67) in a format suitable for the computation of waves travelling at a constant velocity c. This is achieved by looking for solutions of the form

$$\eta_0(x,\tau) = S(\xi), \quad u(x,\tau) = U(\xi) \tag{70}$$

where $\xi = x - c\tau$. Substituting (70) into the system (66)-(67) gives

$$-c\frac{dS}{d\xi} + \frac{dS}{d\xi}U + (S-1)\frac{dU}{d\xi} = 0 \tag{71}$$

$$-c\frac{dU}{d\xi} + U\frac{dU}{d\xi} + B\frac{dS}{d\xi} - E_b\frac{(\epsilon_{f,g}-1)^2}{(1+\epsilon_{f,g}\,\epsilon_{s,f})}\mathcal{H}[S_{\xi\xi}] = -\frac{d^3S}{d\xi^3}. \tag{72}$$

The system (71)-(72) is now solved numerically by finite differences. We assume that the wave is periodic with wavelength λ and symmetric (i.e. $S(\xi+\lambda) = S(\xi)$ and $S(-\xi) = S(\xi)$). We introduce the mesh points

$$\xi_I = \frac{\lambda}{2}\frac{I-1}{N-1} \quad I = 1,\ldots,N, \tag{73}$$

$$\xi_{I+1/2} = \frac{\xi_I + \xi_{I+1}}{2}, \quad I = 1,\ldots,N-1 \tag{74}$$

and the unknowns

$$U_I = U(\xi_I), \quad S'_I = S_\xi(\xi_I), \quad I = 1,\ldots,N. \tag{75}$$

Next we evaluate $U(\xi)$, U_ξ, S_ξ, $S_{\xi\xi}$ and $S_{\xi\xi\xi}$ at the mesh points (74) by four-point difference and interpolation formulae. We evaluate $S(\xi_{I+1/2})$ by integrating S'_I numerically with the condition $S(0) = \alpha$.

We obtain $2N-3$ equations by satisfying (72) at the mesh points (74), $I = 1,\ldots,N-1$ and (71) at the mesh points (74) , $I = 1,\ldots,N-2$. The Cauchy principal value in (72) is evaluated by the trapezoidal rule with a summation over the points (73). Two more equations are obtained by imposing $S'_1 = S'_N = 0$. The last three equations are

$$\int_0^{\lambda/2} S\,d\xi = 0 \tag{76}$$

$$\int_0^{\lambda/2} U\,d\xi = 0 \tag{77}$$

$$S(\xi_1) - S(\xi_N) = h \tag{78}$$

where h is the given amplitude of the wave. Equation (76) fixes the origin of S and (77) defines c. We now have $2N+2$ nonlinear equations for the $2N+2$ unknowns (75), α and c. This system is solved by Newton's method.

We present results for $B = 1$, $E_b = 8$, $\epsilon_{f,g} = 3$, $\epsilon_{s,f} = 0.5$ and $\lambda = 21.7$. Values of c versus h are shown in Figure 3. The horizontal broken line corresponds to the linear approximation (69). As expected the weakly nonlinear results (solid curve) approach the linear solution broken line) as $h \to 0$. Typical profiles are shown in Figure 4. For small values of h the profiles are close to the linear sine profile predicted by the linear theory. However for large values of h, the profiles are clearly nonlinear with sharp crests and broad troughs.

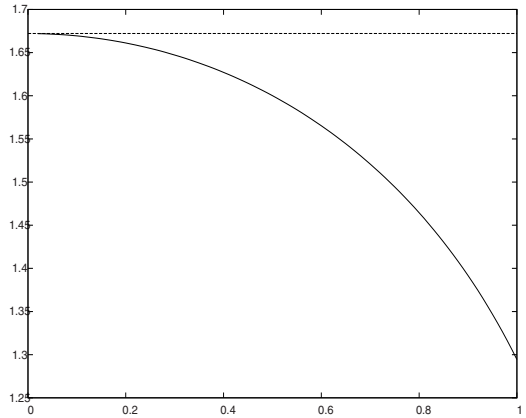

Fig. 3. Values of c versus h for $E_b = 8$, $\epsilon_{s,f} = 0.5$, $\epsilon_{f,g} = 3$ and $\lambda = 21.7$. The solid curve corresponds to the numerical solution of the system (71)-(72). The broken line shows the analytical solution (69).

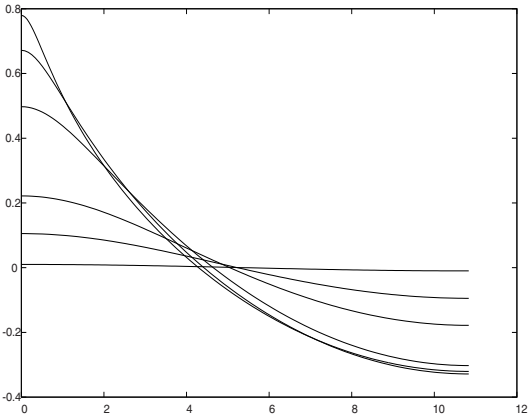

Fig. 4. Wave profiles for $E_b = 8$, $\epsilon_{s,f} = 0.5$, $\epsilon_{f,g} = 3$, $\lambda = 21.7$ and various values of h. Note that half the profile is shown due to symmetry.

6. Conclusions

We have studied the stability and nonlinear dynamics of hanging liquid films that are susceptible to gravitational Rayleigh-Taylor instabilities, under the action of horizontal electric fields applied parallel to the undisturbed fluid interface. Surface tension is retained and the model accounts for the electric field in the block whose underside is wetted by the liquid film, as well as in the air region below the liquid layer (see Figure 1), thus extending the work of Barannyk et al.[13] to configurations that are more likely to be encountered in experiments.

The linear stability of the full problem is studied first. In the absence of an electric field and surface tension, all waves are unstable and in fact the system is short-wave unstable with shorter waves growing the fastest. Surface tension introduces a high-wavenumber regularization and induces a finite band of instability. We establish that the applied electric field has an analogous qualitative effect and acts as a stabilization mechanism. Given any unstable wavenumber, a sufficiently strong electric field will render it linearly stable (these results are in line with previous studies[13]). From a physical perspective this is a useful finding: an externally applied electric field can be used to make relatively thick films stable (i.e. films that are thicker than the capillary length $l_c = \sqrt{\sigma/\rho g}$; for a water-air system $l_c \approx 2\,mm$).

Having established the linear aspects of the problem, we used long-wave theories to develop asymptotically correct one-dimensional model equations to describe the nonlinear dynamics. The analysis results in a system of PDEs coupling the evolution of the interfacial shape and the leading order horizontal velocity in the liquid film. Even though the equations are capable of predicting touchdown events where the liquid layer thins to zero thickness, we have concentrated in situations where the electric field is strong enough to make the system linearly stable. We computed numerically nonlinear traveling waves in such cases and show that connect to the waves predicted by linear theory when the wave amplitudes are small. Such nonlinear coherent structures are useful in enhancing the transport properties of the liquid layer and more detailed studies of such effects would be useful future studies.

Acknowledgements

This work was partly supported by EPSRC grant EP/J019569/1 (JMVB) and the National Science Foundation grant DMS-0707339 (DTP).

References

1. Oron A, Davis SH, Bankoff SG. Long-scale evolution of thin liquid films. *Rev. Mod. Phys.* 1997; **69**:931–980.
2. Craster RV, Matar OK. Dynamics and stability of thin liquid films. *Rev. Mod. Phys.* 2009; **81**:1131–1198.
3. Chang H-C, Demekhin EA. *Complex wave dynamics on thin films.* Amsterdam: Elsevier; 2002.
4. Kalliadasis S, Ruyer-Quil C, Scheid B, Velarde MG. *Falling liquid films*. London: Springer-Verlag; 2012.
5. Tseluiko D, Papageorgiou DT. Wave evolution on electrified falling films. *J. Fluid Mech.* 2006; **556**:361–386.
6. Tseluiko D, Papageorgiou DT. Nonlinear dynamics of electrified thin liquid films. *SIAM J. Appl. Math.* 2007; **67**:1310-1329.
7. Tseluiko D, Papageorgiou DT. Dynamics of an electrostatically modified Kuramoto–Sivashinsky–Korteweg–de Vries equation arising in falling film flows. *Phys. Rev. E* 2010; **82**:016322.
8. Stability of viscous liquid films flowing over topography. *J. Fluid Mech.* 2013; in press.
9. Tseluiko D, Blyth MG, Papageorgiou DT, Vanden-Broeck J-M Electrified viscous thin film flow over topography. *J. Fluid Mech.* 2008; **597**:449-475.
10. Tseluiko D, Blyth MG, Papageorgiou DT, Vanden-Broeck J-M Effect of an electric field on film flow down a corrugated wall at zero Reynolds number. *Phys. Fluids* 2008; **20**:042103.
11. Tseluiko D, Blyth MG, Papageorgiou DT, Vanden-Broeck J-M Viscous electrified film flow over step topography. *SIAM J. Appl. Math.* 2009; **70**:845-865.
12. Tseluiko D, Blyth MG, Papageorgiou DT, Vanden-Broeck J-M Electrified falling-film flow over topography in the presence of a finite electrode. *J. Engng. Math.* 2010; **68**:339-353.
13. Suppression of Rayleigh-Taylor instability using electric fields. *Math. Comp. Simulation* 2012; **82**:1008-1016.
14. Cimpeanu R, Papageorgiou DT, Petropoulos PG. On the control and suppression of Rayleigh-Taylor instability using electric elds. *Phys. Fluids* 2013, submitted.
15. Taylor GI, McEwan AD. The stability of a horizontal fluid interface in a vertical electric field. *J. Fluid Mech.* 1965; **22**: 1–15.
16. Papageorgiou DT, Vanden-Broeck J-M 2004 Large amplitude capillary waves in electrified fluid sheets. *J. Fluid Mech.* 2004; **508**:71-88.